

Supplemental material to "Data-Driven Design of Novel Halide Perovskite Alloys"

Arun Mannodi-Kanakkithodi,^{1, 2, a)} and Maria K. Y Chan^{2, b)}

¹School of Materials Engineering, Purdue University, West Lafayette, Indiana 47907, USA

²Center for Nanoscale Materials, Argonne National Laboratory, Argonne, Illinois 60439, USA

*

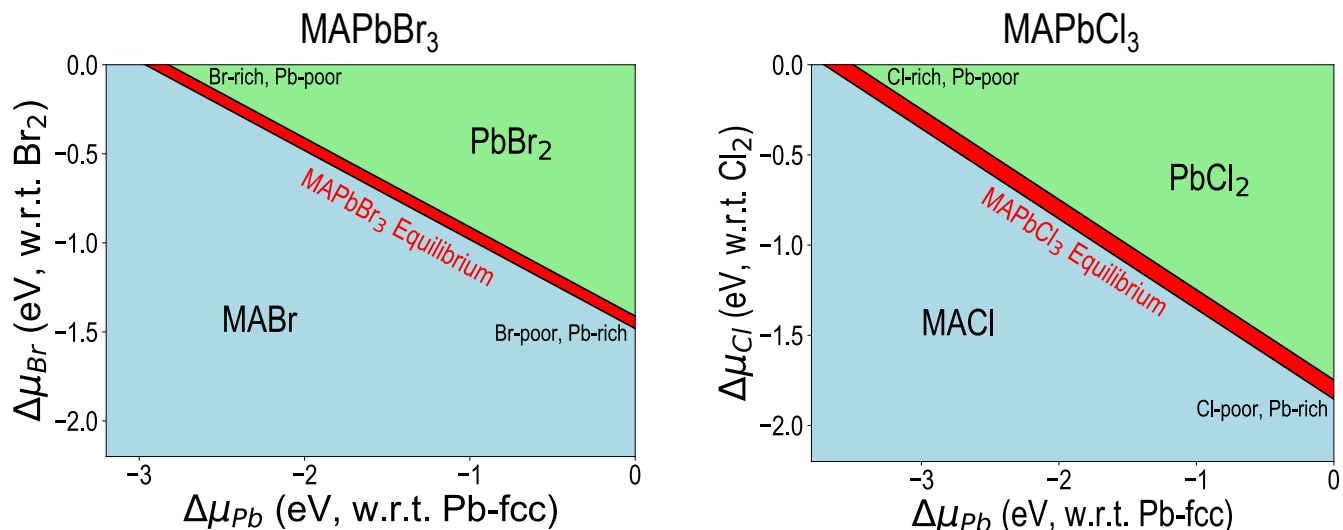


Fig. S1 Calculated chemical ranges of stability for MAPbBr₃ and MAPbCl₃.

Symbol	Ionic_radius (Å)	Boiling_point (K)	Melting_point (K)	Density (g/cc)	Atomic_weight (u)
K	1.51	1033.00	336.80	0.86	39.10
Rb	1.61	961.00	312.63	1.53	85.47
Cs	1.74	944.00	301.54	1.87	132.91
MA	2.17	267.00	180.65	0.70	32.07
FA	2.53	319.00	354.00	1.10	45.06
Ca	1.00	1757.00	1112.00	1.55	40.08
Sr	1.26	1655.00	1042.00	2.54	87.62
Ba	1.42	2078.00	1002.00	3.59	137.33
Ge	0.87	3107.00	1211.50	5.32	72.61
Sn	1.15	2876.00	505.12	7.31	118.71
Pb	1.19	2023.00	600.65	11.35	207.20
Cl	1.81	239.18	172.17	3.21	35.45
Br	1.96	331.85	265.95	3.12	79.90
I	2.20	457.50	386.70	4.93	126.90

Symbol	Electron_affinity (kJ/mol)	Ionization_energy (kJ/mol)	Heat_of_fusion (kJ/mol)	Heat_of_vap (kJ/mol)	Electronegativity
K	48.36	418.80	2.33	76.90	0.82
Rb	46.89	403.00	2.34	69.20	0.82
Cs	45.49	375.70	2.09	67.74	0.79
MA	8.68	926.30	6.13	23.85	2.55
FA	8.60	849.10	6.50	29.00	2.57
Ca	-156.00	589.80	8.53	154.67	1.00
Sr	-168.00	549.50	8.20	136.90	0.95
Ba	-52.00	502.90	8.01	140.20	0.89
Ge	120.00	762.10	31.80	334.30	2.01
Sn	121.00	708.60	7.20	290.37	1.96
Pb	110.00	715.50	4.77	177.90	2.33
Cl	348.80	1251.10	3.21	10.20	3.16
Br	324.60	1139.90	5.29	14.73	2.96
I	295.30	1008.40	7.76	20.90	2.66

Symbol	At_num	Period	Group	Valence	Ox_state
K	19	4	1	1	1
Rb	37	5	1	1	1
Cs	55	6	1	1	1
MA	73	7	1	1	1
FA	91	8	1	1	1
Ca	20	4	2	2	2
Sr	38	5	2	2	2
Ba	56	6	2	2	2
Ge	32	4	14	4	2
Sn	50	5	14	4	2
Pb	82	6	14	4	2
Cl	17	3	17	7	-1
Br	35	4	17	7	-1
I	53	5	17	7	-1

Fig. S2 List of 15 elemental/molecular properties and tabulated values used for each A, B and X-site constituent in the halide perovskite chemical space. All the individual elemental/molecular properties are taken directly or approximated using empirical equations from the references listed below.

References for Elemental/Molecular Properties for Descriptors

- L.Dimesso, A. Quintill, Y.-M. Kim, U. Lemmer, and W. Jaegermann, "Investigation of formamidinium and guanidinium lead tri-iodide powders as precursors for solar cells", Materials Science and Engineering: B, 204, 27–33 (2016) <https://doi.org/10.1016/j.mseb.2015.11.006>.
- <https://pubchem.ncbi.nlm.nih.gov/compound/Methylamine>
- <http://www.chemspider.com/Chemical-Structure.61362.html>
- Ruiying Long, Binghan Li, and Qixi Mi , "Selection of contact materials to p-type halide perovskite by electronegativity matching", AIP Advances 10, 065224 (2020) <https://doi.org/10.1063/5.0008406> .
- <https://webbook.nist.gov/cgi/cbook.cgi?ID=C74895Mask=20>
- <https://webbook.nist.gov/cgi/cbook.cgi?Formula=CN2H6NoIon=onUnits=SI>

Table SI Calculated PV figures of merit (in \log_{10}) for known semiconductors and some selected compounds from the current study.

Compound	\log_{10} (PV FOM)
Si	5.64
SiC	3.76
GaAs	5.66
CdTe	5.46
CdSe	5.31
$\text{CsCa}_{0.25}\text{Ba}_{0.125}\text{Ge}_{0.25}\text{Pb}_{0.375}\text{Cl}_3$	4.72
$\text{MACa}_{0.375}\text{Ge}_{0.5}\text{Pb}_{0.125}\text{Br}_3$	4.88
$\text{MACa}_{0.125}\text{Sr}_{0.125}\text{Ba}_{0.125}\text{Ge}_{0.125}\text{Pb}_{0.5}\text{I}_3$	5.07
$\text{CsCa}_{0.875}\text{Pb}_{0.125}\text{Br}_3$	3.84
$\text{FACa}_{0.125}\text{Sr}_{0.375}\text{Ba}_{0.125}\text{Sn}_{0.125}\text{Pb}_{0.25}\text{I}_3$	4.88

Table SII A comparison of training and test set RMSE values from optimized neural network (NN), random forest (RFR) and Gaussian process regression (GPR) models.

Theory	Property	NN Train	NN Test	RFR Train	RFR Test	GPR Train	GPR Train
PBE	Lattice Constant (Å)	0.09	0.10	0.02	0.05	0.03	0.05
HSE	Lattice Constant (Å)	0.06	0.06	0.03	0.06	0.04	0.05
PBE	Decomposition Energy (eV)	0.05	0.11	0.06	0.12	0.05	0.10
HSE	Decomposition Energy (eV)	0.05	0.09	0.06	0.14	0.05	0.11
PBE	Band Gap (eV)	0.20	0.22	0.09	0.23	0.09	0.25
HSE	Band Gap (eV)	0.19	0.24	0.09	0.20	0.08	0.25
PBE	Refractive Index	0.04	0.05	0.02	0.04	0.03	0.03
PBE	PV FOM (\log_{10})	0.14	0.18	0.04	0.08	0.07	0.10
PBE	X-rich D.F.E. (eV)	0.12	0.23	0.08	0.23	0.14	0.36
PBE	X-rich E_F (eV)	0.06	0.19	0.13	0.25	0.25	0.32
PBE	Medium-X D.F.E. (eV)	0.18	0.29	0.09	0.21	0.16	0.27
PBE	Medium-X E_F (eV)	0.11	0.30	0.08	0.22	0.08	0.26
PBE	B-rich D.F.E. (eV)	0.11	0.30	0.14	0.35	0.22	0.42
PBE	B-rich E_F (eV)	0.11	0.25	0.15	0.33	0.25	0.36
PBE	V_A (0/-1) Transition (eV)	0.07	0.11	0.05	0.11	0.10	0.11
PBE	V_X (+1/0) Transition (eV)	0.19	0.22	0.09	0.21	0.09	0.25

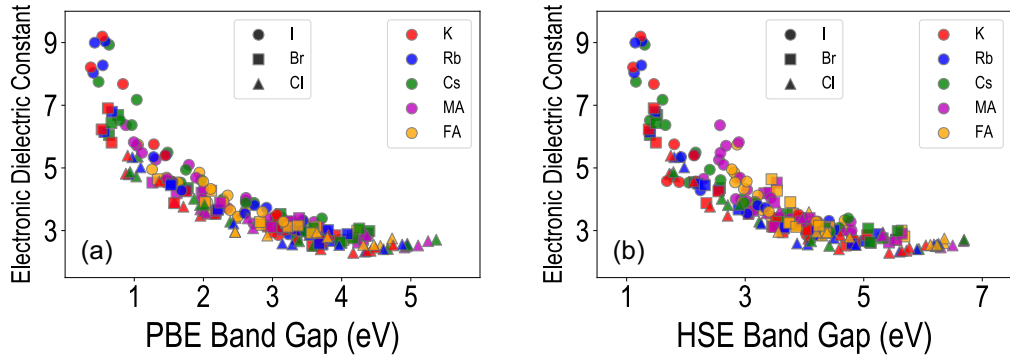


Fig. S3 Electronic component of the dielectric constant plotted against the PBE and HSE band gaps for the DFT dataset of 229 compounds.

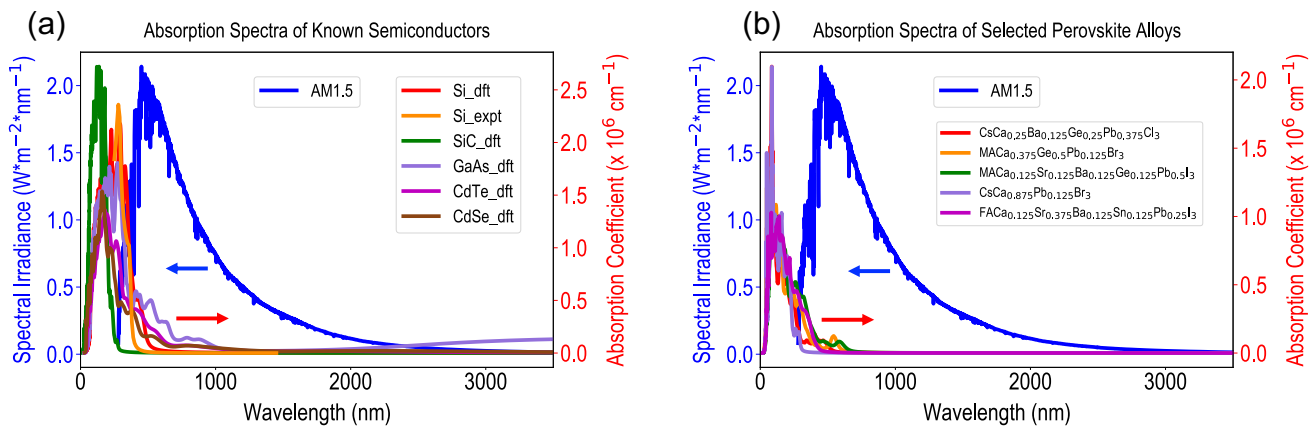


Fig. S4 Computed optical absorption spectra (right y-axis) compared to solar spectral irradiance (left y-axis), for (a) known semiconductors Si, SiC, GaAs, CdTe and CdSe (all in zincblende structures), and (b) selected halide perovskite alloys from the current study. Experimentally measured spectrum is also reported for Si.

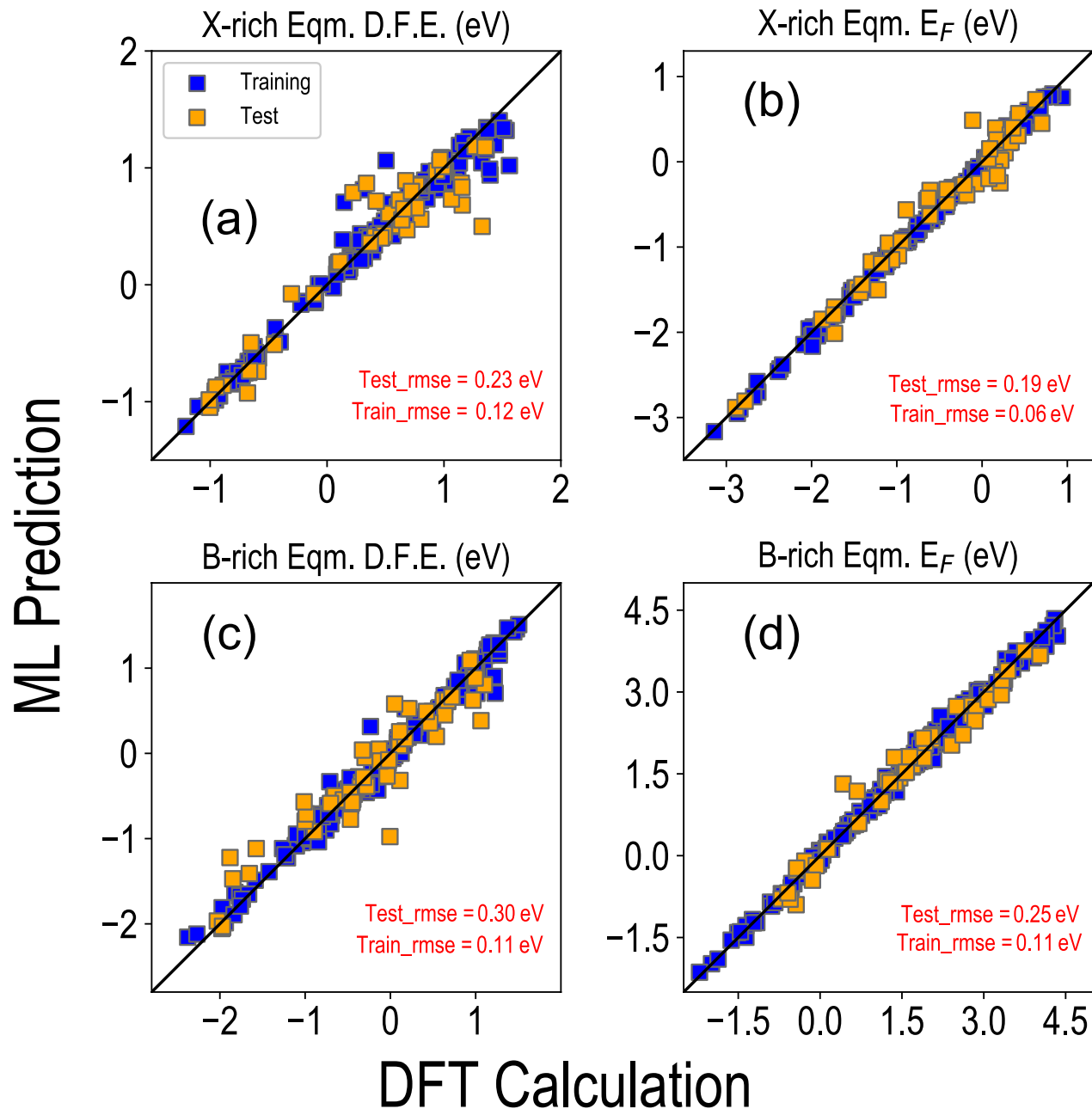


Fig. S5 Optimized NN predictive models for the equilibrium defect formation energy (D.F.E.) and Fermi level (E_F) (as determined by the energetics of A-site and X-site vacancies) at X-rich and B-rich chemical potential conditions. All defect properties are calculated at the PBE level of theory.

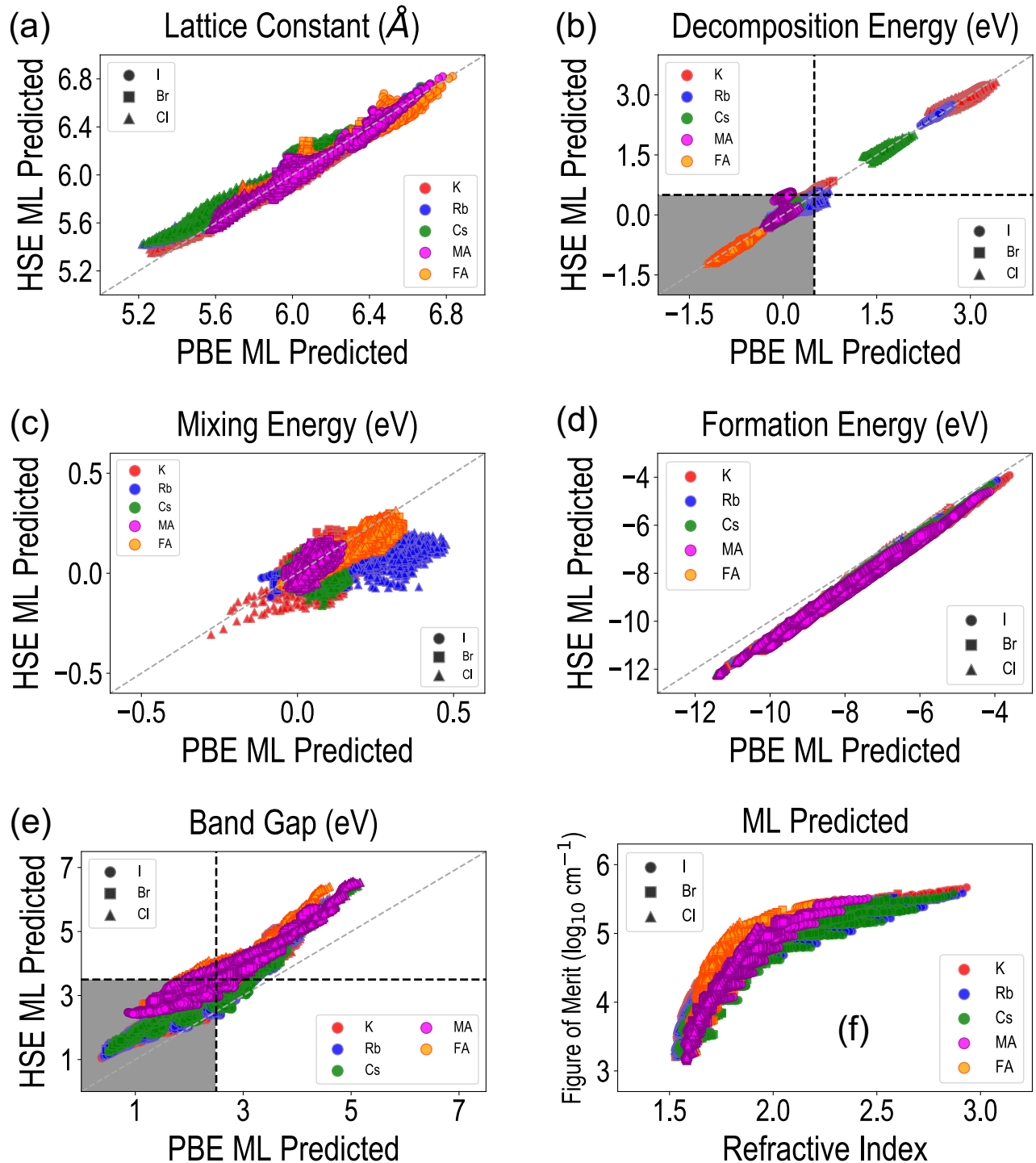


Fig. S6 A visualization of the ML predicted PBE and HSE lattice constants (a), ΔH_{decomp} (b), ΔH_{mix} (c), ΔH_{form} (d), E_{gap} (e), and refractive index vs figure of merit (f), for the chemical space of 17,955 perovskite compounds.

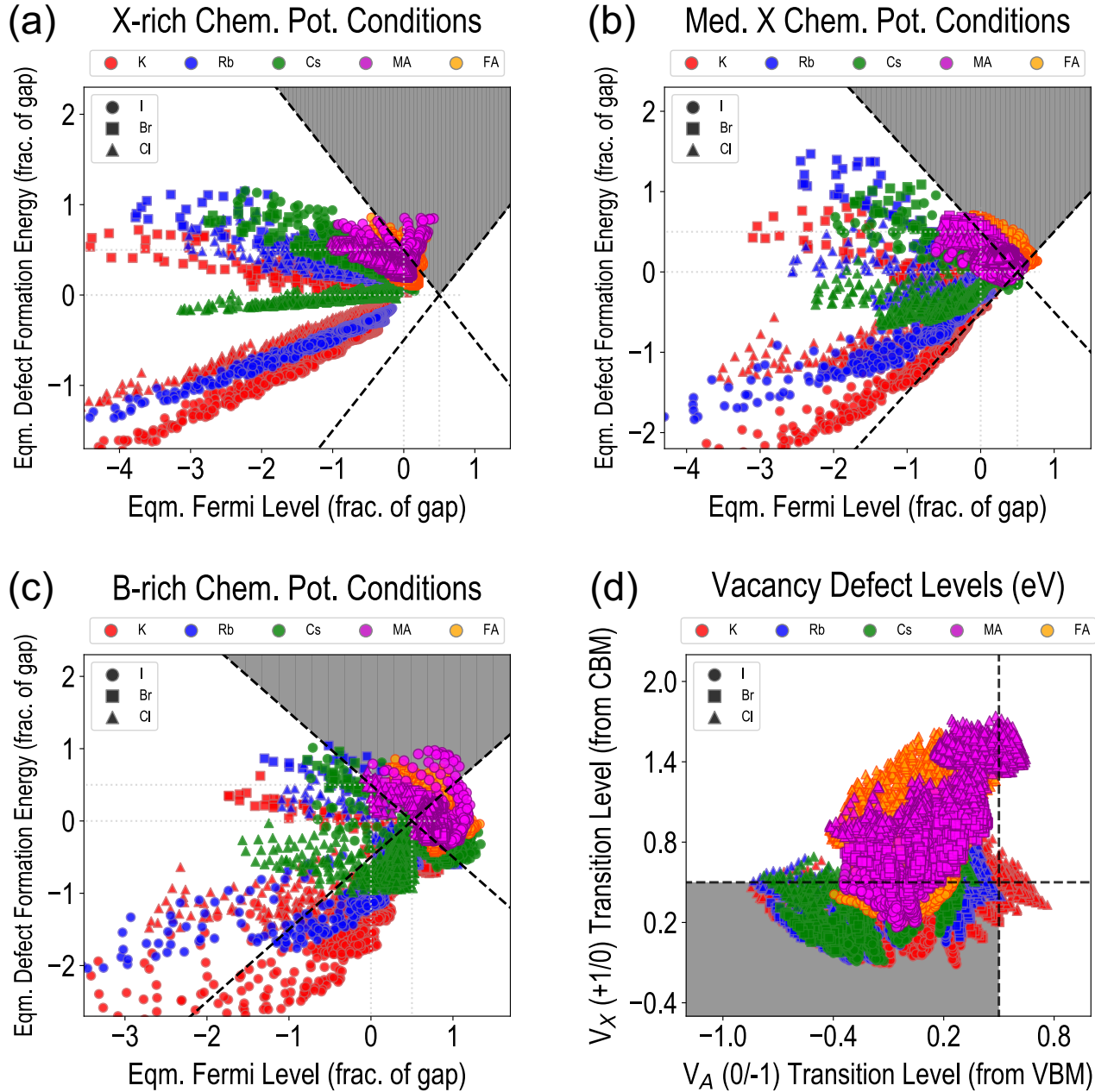


Fig. S7 ML predicted defect properties for the chemical space of 17,955 perovskite compounds: Equilibrium D.F.E. vs E_F/E_{gap} plots are shown for (a) halide rich, (b) medium halide, and (c) B-rich chemical potential conditions. The shaded region represents materials that satisfy the criterion $D.F.E. + E_F/E_{gap} > 1.0$ eV and are thus defect tolerant; for high-throughput screening, this threshold is relaxed to 0.8 eV. The V_A (0/-1) and V_X (+1/0) charge transition levels are plotted in (d), with respect to the VBM and CBM respectively, and the shaded region represents cases with defect levels < 0.2 eV from band edges while the remaining materials have deep vacancy defect levels.

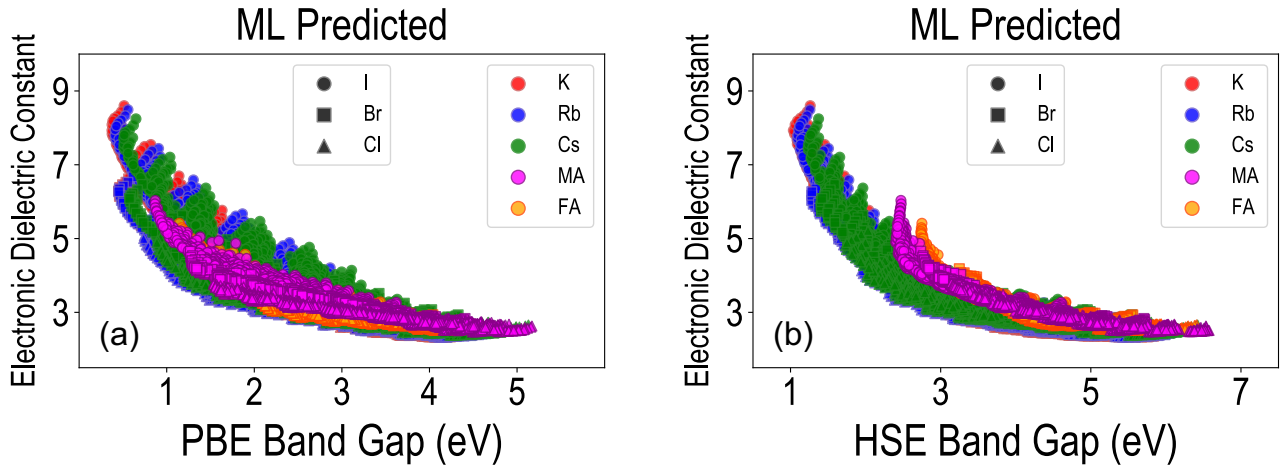


Fig. S8 ML-predicted electronic component of the dielectric constant plotted against the ML-predicted PBE and HSE band gaps for the entire chemical space of 17,955 compounds.

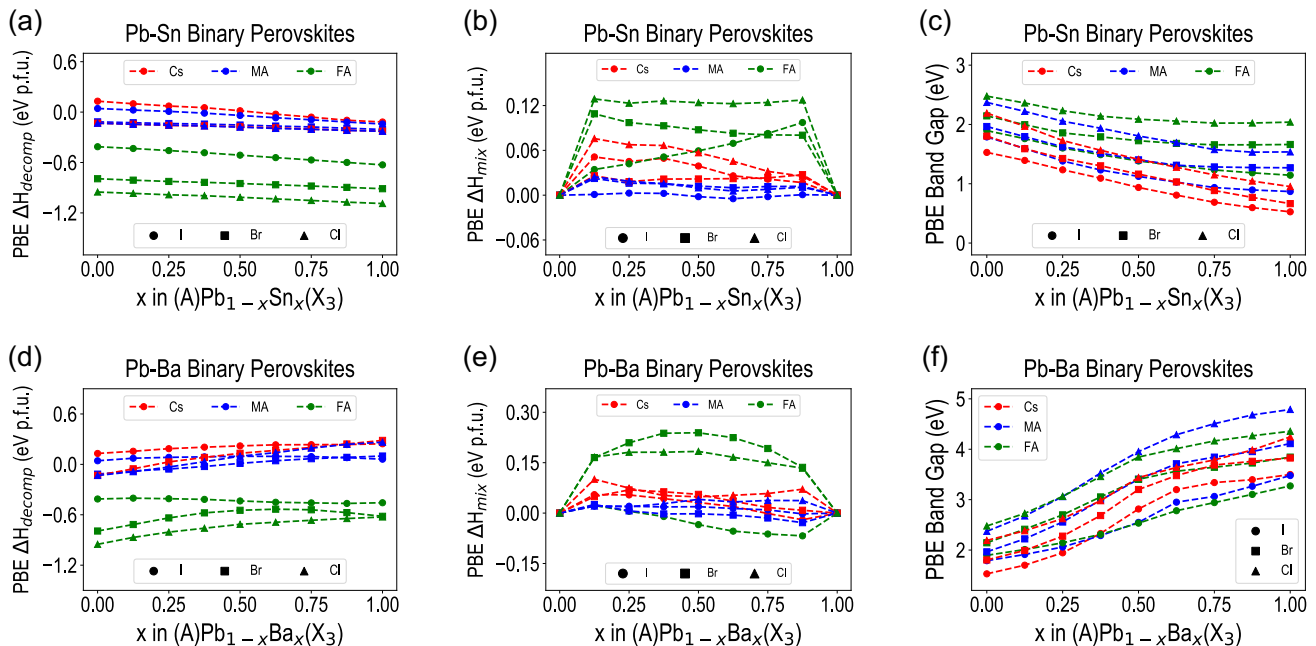


Fig. S9 ML (PBE) predicted decomposition energies, mixing energies (with added entropic contribution) and band gaps of Pb-Sn (a, b, c) and Pb-Ba (d, e, f) binary ABX_3 perovskites with $A = \text{Cs, MA or FA}$ and $X = \text{I, Br or Cl}$, plotted as a function of Sn or Ba content.

Table SIII New compounds used for testing out-of-sample predictive power.

Data Type	Perovskite Formula	DFT-PBE ΔH_{decomp} (eV p.f.u.)	DFT-PBE E_{gap} (eV p.f.u.)	ML-PBE ΔH_{decomp} (eV)	ML-PBE E_{gap} (eV)
New A/X site mixed	$K_{0.125}FA_{0.875}SnBr_3$	-0.83	1.60	-0.87	1.36
New A/X site mixed	$MA_{0.5}FA_{0.5}CaCl_3$	-0.32	4.31	-0.42	4.74
New A/X site mixed	$Rb_{0.125}Cs_{0.875}CaBr_3$	-0.20	4.31	-0.15	4.44
New A/X site mixed	$K_{0.5}MA_{0.5}SnBr_3$	-0.09	1.54	-0.13	0.51
New A/X site mixed	$Rb_{0.375}Cs_{0.625}GeBr_3$	-0.22	0.72	-0.24	0.70
New A/X site mixed	$MACa_{0.125}Pb_{0.875}Br_{1.5}Cl_{1.5}$	-0.13	2.43	-0.16	2.29
New A/X site mixed	$MASr_{0.125}Pb_{0.875}Br_{1.5}Cl_{1.5}$	-0.13	2.47	-0.15	2.36
New A/X site mixed	$MABa_{0.125}Pb_{0.875}Br_{1.5}Cl_{1.5}$	-0.10	2.50	-0.15	2.40
New A/X site mixed	$MAGe_{0.125}Pb_{0.875}Br_{1.5}Cl_{1.5}$	-0.16	2.18	-0.23	1.97
New A/X site mixed	$MASn_{0.125}Pb_{0.875}Br_{1.5}Cl_{1.5}$	-0.16	1.98	-0.23	1.97
New A/X site mixed	$CsPbI_{0.375}Br_{2.625}$	-0.12	1.69	-0.18	1.70
New A/X site mixed	$MASrBr_{1.125}Cl_{1.875}$	0.02	4.73	-0.02	4.79
New A/X site mixed	$FAGeBr_{2.625}Cl_{0.375}$	-1.01	2.91	-0.97	2.36
New A/X site mixed	$RbSnBr_{2.625}Cl_{0.375}$	-0.05	0.58	-0.12	0.67
New A/X site mixed	$MASnI_{2.25}Br_{0.75}$	-0.13	1.09	-0.19	0.91
New B-site Element	$MAPb_{0.875}Be_{0.125}I_3$	0.15	1.82	0.06	1.51
New B-site Element	$MAPb_{0.875}Mg_{0.125}I_3$	0.08	1.89	0.06	1.66
New B-site Element	$MAPb_{0.875}Si_{0.125}I_3$	0.11	1.48	0.06	1.52
New B-site Element	$MAPb_{0.875}Zn_{0.125}I_3$	0.12	1.35	0.04	1.70
New B-site Element	$MAPb_{0.875}Cd_{0.125}I_3$	0.05	1.41	0.04	1.80
New B-site Element	$MAPb_{0.875}Be_{0.125}Br_3$	0.05	2.16	-0.15	1.87
New B-site Element	$MAPb_{0.875}Mg_{0.125}Br_3$	-0.06	2.11	-0.13	1.99
New B-site Element	$MAPb_{0.875}Si_{0.125}Br_3$	-0.02	1.74	-0.17	1.85
New B-site Element	$MAPb_{0.875}Zn_{0.125}Br_3$	-0.03	2.19	-0.16	1.91
New B-site Element	$MAPb_{0.875}Cd_{0.125}Br_3$	-0.06	1.74	-0.16	1.99
New B-site Element	$MAPb_{0.875}Be_{0.125}Cl_3$	-0.17	2.65	-0.18	2.44
New B-site Element	$MAPb_{0.875}Mg_{0.125}Cl_3$	-0.14	2.62	-0.17	2.58
New B-site Element	$MAPb_{0.875}Si_{0.125}Cl_3$	-0.08	2.10	-0.23	2.42
New B-site Element	$MAPb_{0.875}Zn_{0.125}Cl_3$	-0.09	2.64	-0.19	2.47
New B-site Element	$MAPb_{0.875}Cd_{0.125}Cl_3$	-0.17	2.24	-0.18	2.53
$3 \times 3 \times 3$ supercell alloy	$MAPb_{0.96}Ba_{0.04}I_3$	0.04	1.61	0.06	1.81
$3 \times 3 \times 3$ supercell alloy	$MAPb_{0.93}Sn_{0.07}I_3$	0.02	1.50	0.05	1.68
$3 \times 3 \times 3$ supercell alloy	$MAPb_{0.96}Sn_{0.04}Br_3$	-0.14	1.84	-0.16	1.95
$3 \times 3 \times 3$ supercell alloy	$MAPb_{0.93}Sn_{0.035}Ba_{0.035}Br_3$	-0.13	1.93	-0.14	2.02
$3 \times 3 \times 3$ supercell alloy	$MAPb_{0.89}Sr_{0.11}Br_3$	-0.12	2.18	-0.11	2.20

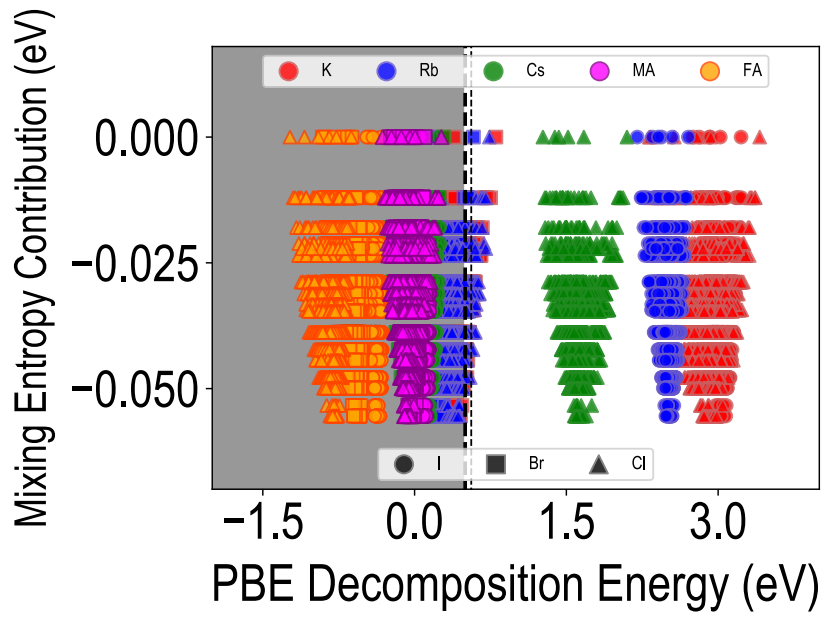


Fig. S10 Energy contribution from mixing entropy of halide perovskite alloys plotted against ML-predicted PBE decomposition energies.

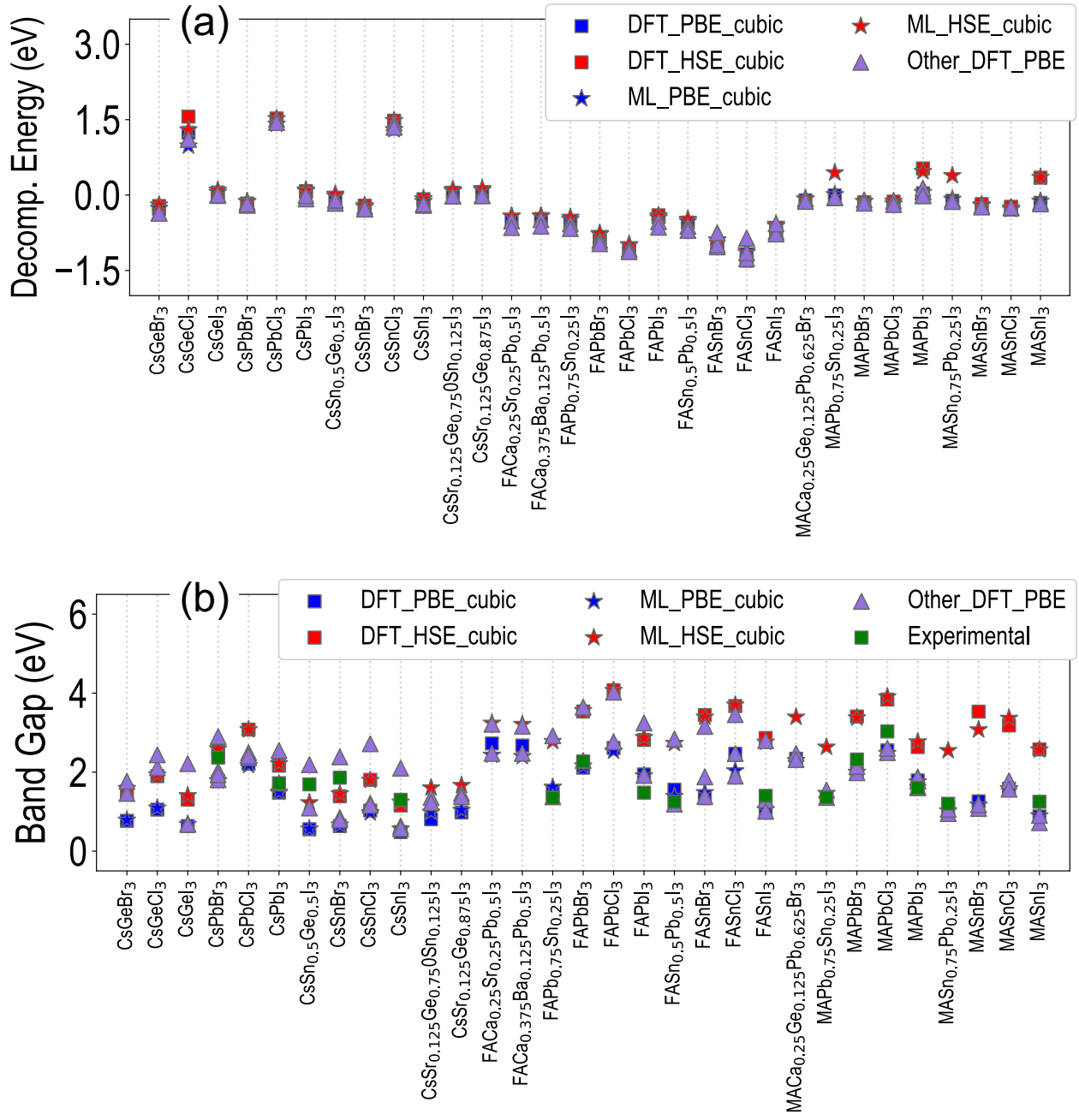


Fig. S11 Effect of perovskite structure on computed properties: (a) Decomposition energies and (b) band gaps for cubic phases at the PBE- and HSE-level from DFT/ML are compared with PBE predicted values for non-cubic phases, for a total of 31 compounds labeled on the x-axis.

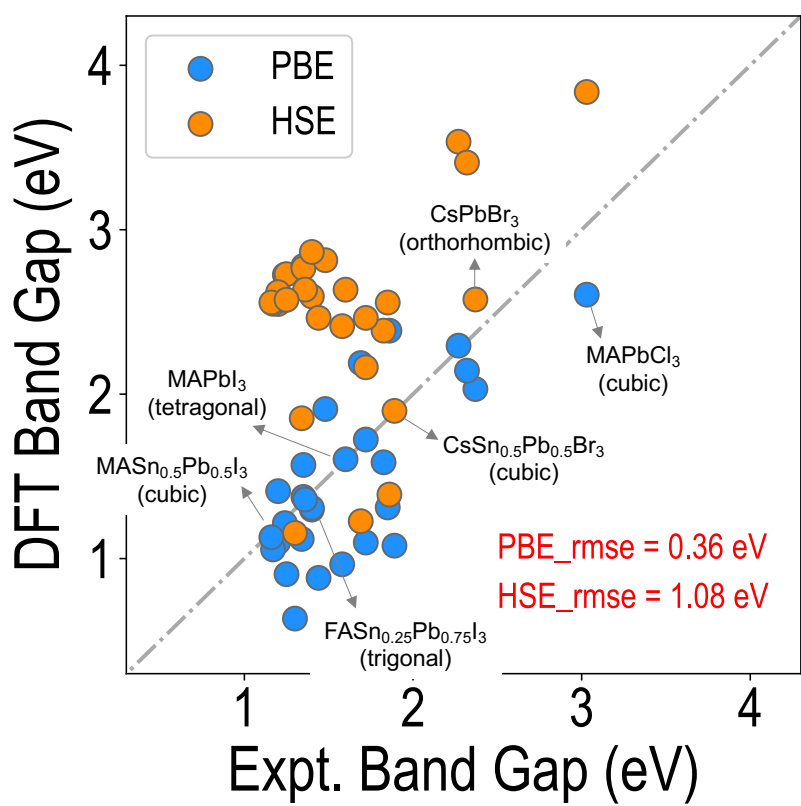


Fig. S12 PBE- and HSE-level estimates of band gap compared with collected experimental measurements for 36 compounds.